Dephosphorization Kinetics between Bloated Metal Droplets and Slag Containing FeO: The Influence of CO Bubbles on the Mass Transfer of Phosphorus in the Metal

Kezhuan Gu, Neslihan Dogan and Kenneth S. Coley

McMaster Steel Research Centre
Department of Materials Science and Engineering
McMaster University
1280 Main Street West, Hamilton, Ontario, Canada, L8S 4L7
Email: guk3@mcmaster.ca and coleyk@mcmaster.ca

Keywords: Bloated Metal Droplets, Dephosphorization Kinetics, CO bubble, Surface Renewal, Mass Transfer

ABSTRACT

Dephosphorization kinetics of bloated metal droplets was investigated in the temperature range from 1813K (1540°C) to 1913K (1640°C). The experimental results showed that the overall mass transfer coefficient,k_o, decreased with increasing temperature because of decreasing phosphorus partition ratio, L_P. It was also found that the mass transfer coefficient for phosphorus in the metal, k_m, had the highest value at the lowest temperature (*i.e.*, 1813K (1540°C)) because the formation of smaller CO bubbles increased the rate of surface renewal, leading to faster mass transport. Meanwhile, metal droplets without carbon were also employed to study the effect of decarburization on dephosphorization. The results show that although decarburization lowers the driving force significantly, k_m (6.2×10^{-2} cm/s) for a carbon containing droplet is two orders of magnitude higher than that for carbon free droplets (5.3×10^{-4} cm/s) because of the stirring effect provided by CO bubbles. This stirring offers a faster surface renewal rate, which surpasses the loss of driving force and then leads to a faster dephosphorization rate.

I. INTRODUCTION

In basic oxygen steelmaking, metal droplets created by the impact of the oxygen jet are ejected into the slag, where they are decarburized and dephosphorized by reaction with iron oxide. Those droplets which swell because of internal nucleation of CO bubbles are termed bloated droplets.The behavior of bloated droplets in terms of decarburization has been studied extensively, [1-7] although several of these studies predate the coining of the term "bloated droplet" which was first used by researchers in the authors' laboratory. [8] Models for predicting residence time in the emulsion zone of the BOF based on droplet bloating behavior have also been developed. [8, 9] Workers at Swinburne University in Australia [10, 11] have developed an overall BOF model considering the behavior of bloated droplets. The development of the bloated droplet concept and its influence on BOF modeling has recently been reviewed in detail by Brooks *et al*. [12] All of these studies were focused on decarburization kinetics and the causes of droplet swelling. There are very few studies on bloated droplet refining kinetics related to elements other than carbon. One example of this is dephosphorization, which occurs in competition with decarburization in the emulsion zone of the BOF. Based on pilot plant data, Hewage *et al*. [13] attempted to model dephosphorization in the

emulsion zone however these workers found that dephosphorization could not be explained by a simple first order equation with either static equilibrium or dynamic equilibrium values, due to the transient behavior of rate parameters such as instantaneous area, residence time and mass transfer coefficient. It is well established that dephosphorization is controlled by mass transfer in the metal, slag or both simultaneously. Therefore, it should be possible to describe the reaction using a rate equation that is first order with respect to phosphorus concentration in the metal. The terms dynamic and static used by Hewage *et al*. [13] refer to the equilibrium partition of phosphorus which exists at the slag metal interface. It is common practice in kinetic studies to assume that this value is constant; static equilibrium. This approach is often adequate, however, the oxygen potential at the interface will change with time, because of changes in the balance between oxygen supply and consumption; dynamic oxygen potential. Although equilibrium with respect to phosphorus is maintained at the slag metal interface, this equilibrium is set by the oxygen potential which changes with time, leading to a changing or dynamic equilibrium with respect to phosphorus. The concepts of dynamic oxygen potential and dynamic equilibrium with respect to phosphorus, have been discussed in detail in previous work by the authors [14] and others [15]. This becomes important when dephosphorization is accompanied by oxidation of elements which have a higher affinity for oxygen. This concept is used in Section IV-B of this paper.

In order to obtain a better understanding of dephosphorization kinetics during decarburization, more detailed work is needed. There is common agreement on some aspects of dephosphorization kinetics associated with decarburization. Firstly, droplet swelling, caused by CO formation inside the droplet increases the droplet residence time in the slag. Secondly, longer residence time favors refining reactions, especially for dephosphorization which can only take place at a significant level when metal is in contact with slag. Thirdly, decarburization will suppress dephosphorization by competing for oxygen, thereby lowering the interfacial oxygen potential [14-19] which controls the driving force for dephosphorization. Finally, because of droplet swelling, the slag/metal interfacial area will change with time; this must be accommodated in the rate equation.

The influence of decarburization on the thermodynamic driving force for dephosphorization has been investigated in detail, [14-19] but the detailed effect of decarburization on the kinetics of dephosphorization is not fully understood, especially the stirring effect introduced by CO bubbles. In the present study, the role of CO bubbles on dephosphorization kinetics is investigated in detail.

II. EXPERIMENTAL PROCEDURE

A resistance heated vertical tube furnace (see Figure 1), with an 80mm diameter alumina working tube was used. The furnace was equipped with, X-ray imaging to observe the swelling of droplets in-situ, and a pressure transducer with maximum measurable range of 13.8 kPa to measure gas evolution using the constant volume pressure increase technique (CVPI). This technique measures the pressure change caused by gas evolution during reaction, the measured pressure is converted to moles of CO evolved through calibration before each experiment. By injecting known volumes of gas at the temperature of interest, the conversion coefficient between pressure changes read from pressure transducer and moles of gas can be determined. This was then used to calculate the total CO generation during the reaction. The measured decarburization data from the pressure transducer was also compared with LECO analysis for carbon, of post reaction samples. These analyses showed reasonable agreement with a difference less than 10 pct of the measured value.

Experiments were conducted in the temperature range from 1813K (1540ºC) to 1913K (1640 ºC). Three types of droplet were used in this study, *i.e.*, carbon containing droplets with two sulfur contents: Fe-2.62 wt pct C-0.088 wt pct P-0.007 wt pct S, and Fe-2.62 wt pct C-0.088 wt pct P-0.014 wt pct S, as well as carbon free droplets Fe-0.088 wt pct P-0.007 wt pct S. The different sulfur contents were used, because previous work in the authors' laboratory [19] has shown that sulfur has a strong influence on CO formation rate; the rate initially increases to a peak at 0.014 wt pct S. Thus, by using droplets with different sulfur contents, it was possible to determine the mass transfer coefficient of phosphorus at two CO bubbling rates. The carbon free droplet allowed the mass transfer coefficient to be determined in the absence of CO bubbling.

A slag of 25±0.5 g, composed of 32 wt pct CaO-35 wt pct SiO_2-17 wt pct Al_2O_3-16 wt pct FeO, was placed in a 45 mm diameter alumina crucible located in the hot zone of the furnace and was melted under an argon atmosphere. High-purity argon was used during the experiments. Before entering the reaction tube, the argon was passed through a gas purifying system consisting of columns filled with anhydrous $CaSO_4$ (drierite) and a furnace containing copper turnings running at 873K (600 °C). Prior to the start of each experiment the furnace was evacuated using a vacuum pump and back filled with argon, this process was repeated three times prior to completely sealing the furnace and starting the experiment. During the preparation of the atmosphere, the crucible containing slag was held in the hot zone of the furnace. The droplet was held by a magnet at the top of the furnace, inside an alumina tube which was sealed from the outside atmosphere. To start the experiment, the droplet was released by removing the magnet. It then fell into the slag via a small hole at the bottom of the alumina tube. The hole in the tube was sized to ensure the droplet was molten before entering the slag. The reaction time was set to zero when the droplet was observed, by X-ray, to fall into the slag. Samples were quenched at different reaction times and taken for chemical analysis of phosphorous using Inductively Coupled Plasma Optical Emission Spectroscopy (ICP-OES). Optical microscopy was also employed to reveal the presence of cavities (the remnants of bubbles) inside quenched droplets after reaction. The rod used to support the alumina crucible in the hot zone of the furnace was held in place by an O-ring and a collar at the base of the furnace. By releasing the collar, the crucible could be dropped from the hot zone into the quench chamber (water cooled stainless steel) within 1 second.

The experimental technique was limited by a very short reaction time which restricted the collection of data to describe the reaction kinetics in detail. Because of these limitations, the authors would not have chosen this technique to study generic dephosphorization behavior. However, in the present case the focus was on the interplay between decarburization and dephosphorization in bloated droplets thereby limiting the authors to study bloated droplets.

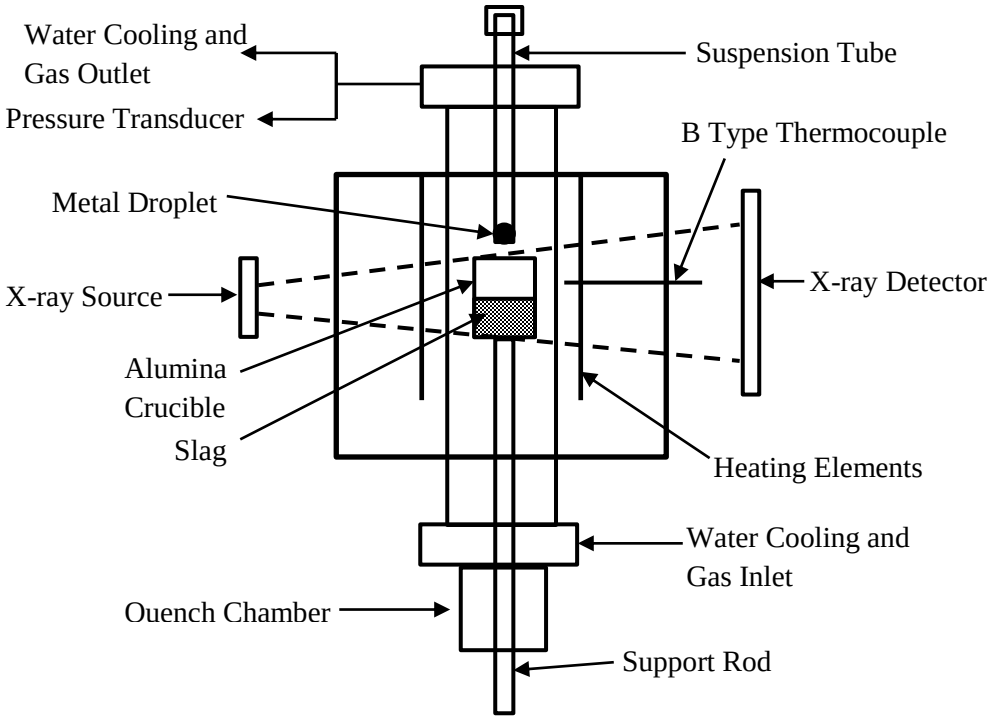

Fig. 1—Schematic diagram of the furnace.

III. EXPERIMENTAL RESULTS

A. Decarburization as a Function of Temperature

Figure 2(a) shows the total amount of CO generated for 0.007 wt pct S droplets as a function of time and temperature in the range from 1813 K (1540 °C) to 1913 K (1640 °C). Figure 2(b) shows similar data for 0.014 wt pct S droplets at 1853 K (1580 °C) and 1913 K (1640 °C). All plots shown in Figure 2 show the same characteristic shape; an initial "incubation period" where the reaction is relatively slow, followed by a period of much faster relatively constant rate, after which the rate tails off. Strictly speaking, the incubation period could more properly be described as a period of mixed internal-external decarburization, as during this period CO gas is formed at the slag/metal interface as well as inside the droplet. The period of much faster reaction following the incubation period, coincides with a shift to internal nucleation of CO which leads to droplet swelling or bloating. In the current paper, the initial period of slow reaction will be referred to as the incubation period despite the fact the decarburization reaction is already well established at the surface of the droplet. These figures also show that the decarburization rate increases with increasing temperature. The maximum slope of each curve shown in Figure 2(a) was taken as the peak CO evolution rate. Based on calibration by injection of known volumes of gas and by comparing the measured decarburization with the cumulative total, the CO evolution measurements are precise to ±10 pct. And the error for the determination of peak decarburization rate is ±7 pct.

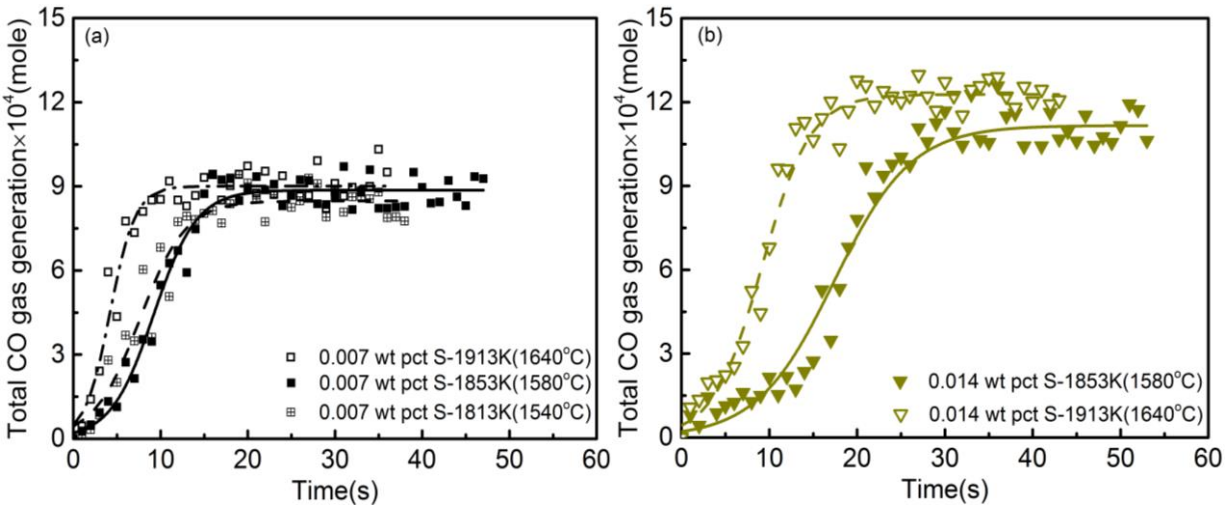

Fig. 2—Decarburization behavior of droplets: CO gas generation with time for (a) 0.007 wt pct S droplets, (b) 0.014wt pct S droplets.

The volume of CO generated in normal cubic meters is determined using the constant volume pressure increase technique. The CO/CO2 ratio in equilibrium with the activity of FeO in the current slag ranges from 15.7 to 18.4 within the temperature range in this study. Assuming all the gas formed is CO introduces no error to the decarburization rate, but will introduce a small error to the calculated FeO depletion (±6 pct). One may therefore calculate the carbon removed from the pressure transducer data, and the FeO content of the slag by mass balance with carbon. It is worth noting that the authors have analyzed the post reaction samples for carbon and they agree fairly well with the results obtained from pressure transducer (±10 pct of carbon content). The slag composition was chosen near alumina saturation, and from slags that have been measured the maximum alumina pickup was less than 3 wt pct, which would decrease the phosphorus partition by about 15 pct over the total time of reaction. A difficulty in attributing composition to the part of the slag involved in the reaction arises because the slag partitions into a dense slag and a foamy slag. Once the droplet rises into the foamy slag all the stirring is above the dense slag so one can expect little mixing of the two layers. The authors have managed to obtain separate analyses for dense and foamy slag in several cases. This data shows that for samples taken after the intense period of decarburization the FeO in the foamy slag has been depleted to about 75 pct of the original content. Consequently, the authors have chosen to use the decarburization data and the residence time in either the foamy slag or the dense slag, to calculate the FeO depletion. This methodology is reflected in the development of equations from A1, to A2 and A3 described in the Appendix.

B. Droplet Swelling behavior at Different Temperatures

By inspecting the recorded X-ray videos the change in the volume of droplets was determined as a function of time and temperature, as shown in Figure 3 for 0.007 and 0.014 wt pct S droplets. Figure 3(a) shows that the incubation time for droplet swelling decreases from 8 seconds to

approximately 2 seconds as temperature increases from 1813 K (1540 °C) to 1913 K (1640 °C) for 0.007 wt pct S droplets. The change in incubation time can be explained by surface poisoning of oxygen dissolution by sulfur. This effect weakens as the temperature increases because sulfur becomes less surface active at higher temperatures. [20-22] Similar behavior is observed for droplets with 0.014 wt pct S shown in Figure 3(b). Inspection of Figure 2 shows that the formation of CO goes through a slower period during the early stages of reaction. Comparison with Figures 3(a) and (b) shows that this slower period represents an "incubation period" for droplet swelling. This period has been attributed in the authors' previous work to the time for the oxygen concentration in the droplet to build up and the internal nucleation of CO to become fully established. [6, 7, 23]

The volume for carbon free droplets (0.007 wt pct S) at 1853 K (1580 °C) was also plotted against time in Figure 3(c), showing that the volume of carbon free droplets remains relatively constant throughout the course of the experiment. This is expected due to the absence of CO evolution inside droplet. It is worth noting that although the shape of carbon free droplet was not changed significantly during reaction, it oscillated horizontally. This type of interfacial phenomena was somehow different from the emulsification observed in the case of carbon free liquid iron by Manning and Fruehan, [24] Assis *et al.* [25] and Spooner *et al.* [26] The difference in behavior probably arises from the lower basicity slag employed in the present study; (wt pct CaO/wt pct SiO_2= 0.9) in the current work and between 1.7 and 3 in the work of Manning and Fruehan, [24] Spooner *et al.* [26] and Assis *et al.* [25] Assis *et al.* [25] and Spooner *et al.* [26] also employed slag with Fe_tO higher than 30 wt pct compared with 16 wt pct FeO employed in current study.

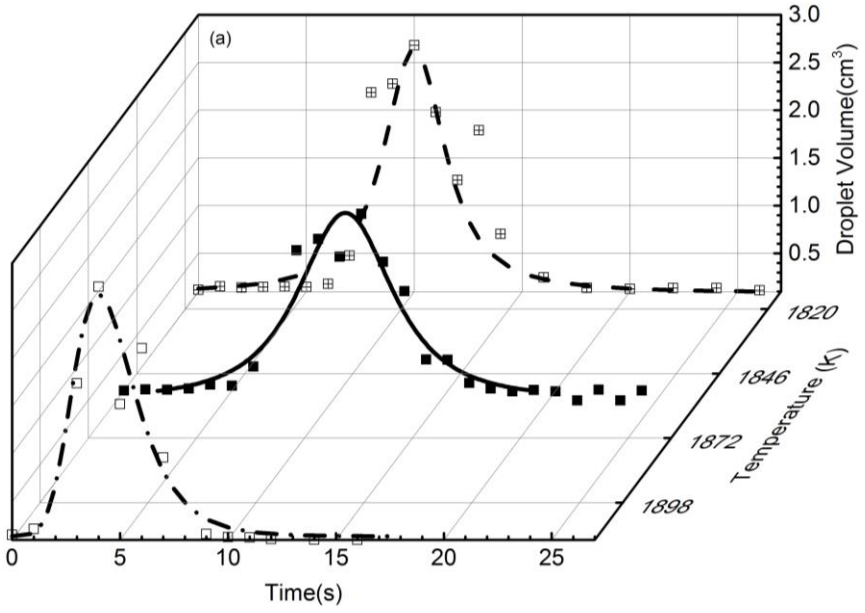

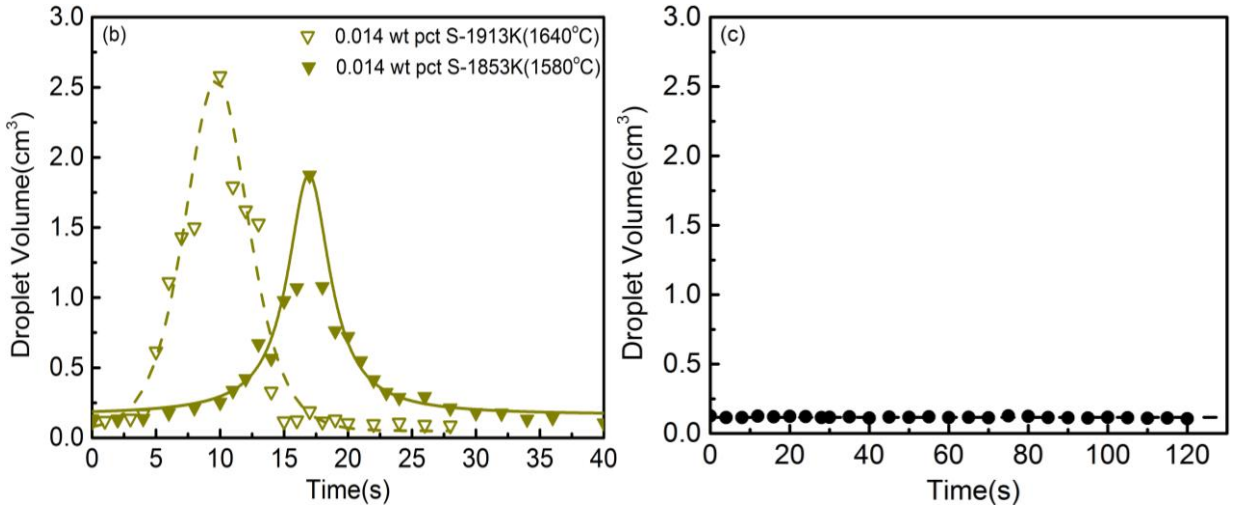

Fig. 3—Swelling behavior of droplets: (a) 0.007 wt pct S droplets at different temperature, (b) 0.014 wt pct S droplets at different temperature and (c) C-free droplets (0.007 wt pct S) at 1853K (1580°C).

For the relatively short reaction times which are the focus of this study, the mass of the droplet after an experiment is between 82 and 90 percent of the original mass. The diameter based on X-ray images ranges, over the course of an experiment, between 100 and 300 percent of the original. Quenched droplets are typically slightly larger than the original because of retained gas, shown in Figure 6. Instead of measuring these parameters for every experiment, the authors determine the size of droplets as a function of time based on X-ray videos. It is worth noting that while the mass loss of the droplet may be interesting, it is difficult to be certain when and how the mass loss has occurred. From X-ray videos one can see a small number of extremely small metal droplets breaking away due to bubbles bursting through the surface. It is also known that the bloated droplets collapse during rapid cooling and it is believed that some of the droplet may break off at that point. The authors have accepted this uncertainty in the data, primarily because of the difficulty of quantifying the timing and the precise role of each mechanism of mass loss. This approach appears to be justified within the limitations of the technique, as the carbon content of metal droplets measured from LECO analysis agrees well with that determined from pressure transducer measurements (±10 pct of carbon content).

C. Dephosphorization of Droplets with and without Carbon

The change of phosphorous content in metal droplets as a function of time for 0.007 and 0.014 wt pct S droplets at different temperatures is shown in Figure 4. Figure 4(a), (b) and (c) show the dephosphorization behavior of 0.007 wt pct S droplets; all exhibit a complex dephosphorization-reversion-renewed dephosphorization behavior depending on their movement between the dense and foamy slag. This can be explained if one considers the difference of liquid volume and mass transfer coefficient between foamy slag and dense slag. Droplets are initially dephosphorized and at some point the oxygen potential at the interface is lowered to the extent that phosphorus is reduced back into the metal. This may occur because if a sudden increase in the rate of carbon

oxidation, or because the slag becomes depleted in FeO. In the current case when droplet bloating is initiated, the decarburization rate increases dramatically, then the droplet rises into the foamy slag. The smaller liquid slag volume in the foamy slag leads to more rapid depletion of FeO. The increase in the decarburization rate and the depletion of FeO may contribute to the phosphorus reversion. However, the extent of reversion will be limited by the liquid slag volume in the foam. When the decarburization rate subsides and the droplet sinks back into the dense slag, the droplet is reintroduced to a higher FeO slag. This higher FeO slag and the slower decarburization rate, will cause an increase in the interfacial oxygen potential which may result in renewed dephosphorization. Droplets with 0.014 wt pct S show a similar behavior to 0.007 wt pct S droplets as seen in Figures 4(e) and (f).

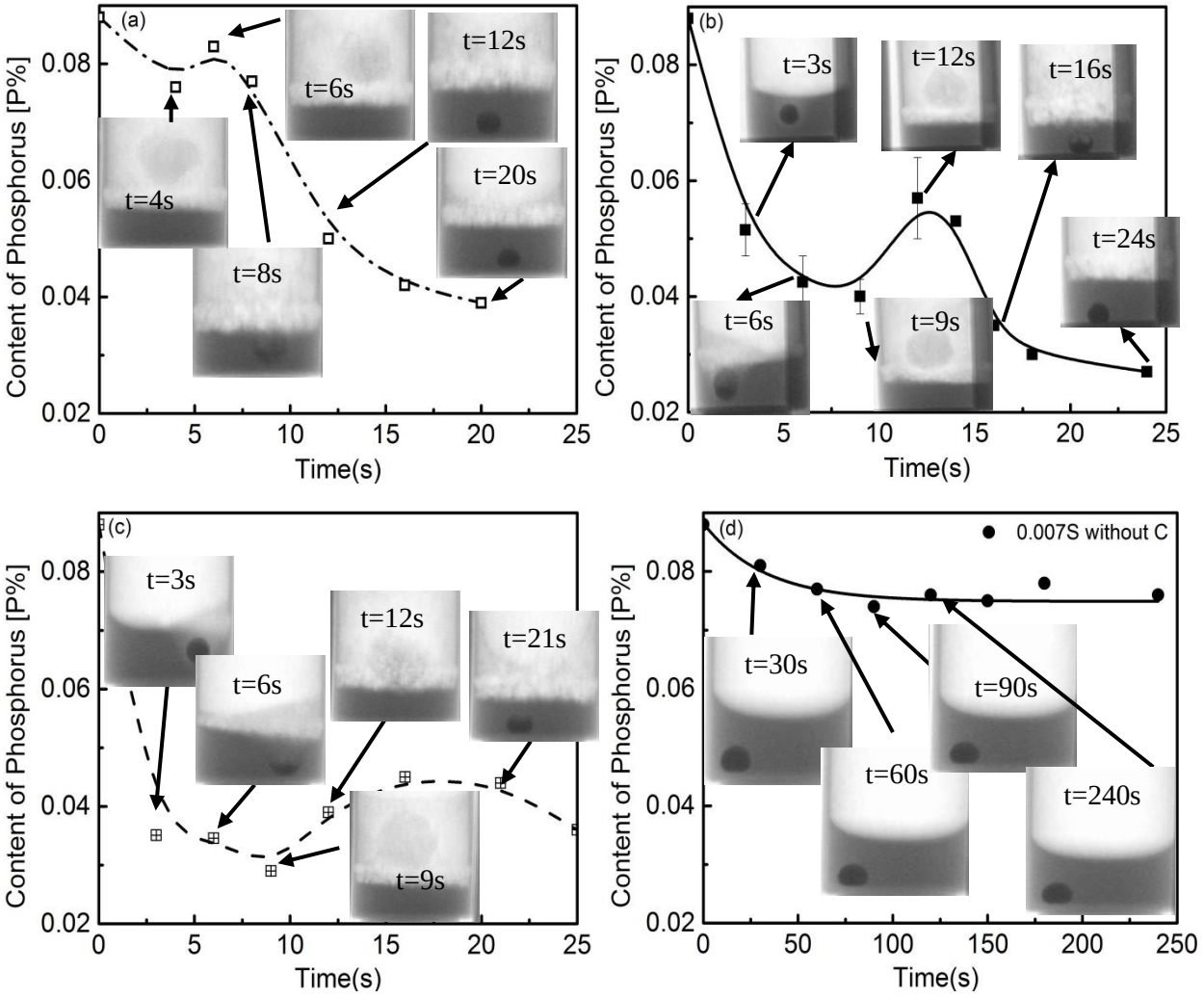

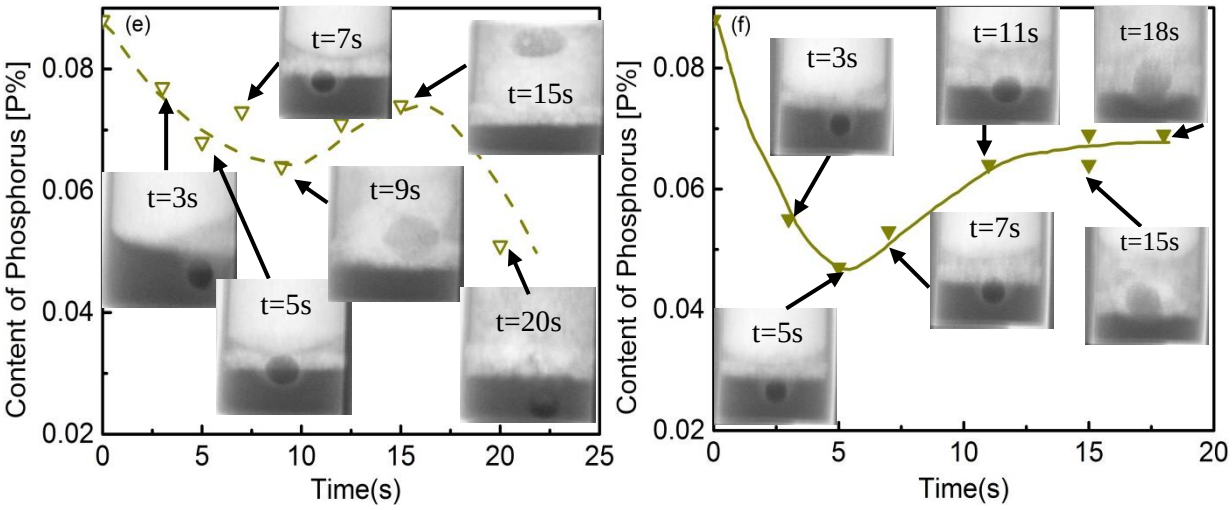

Fig. 4—Plot of dephosphorization as a function of time and temperature: (a) 0.007 wt pct S at 1913 K (1640 °C), (b) 0.007 wt pct S at 1853 K (1580 °C), (c) 0.007 wt pct S at 1813 K (1540 °C), (d) 0.007 wt pct S C-free droplet at 1853 K (1580 °C), (e) 0.014 wt pct S at 1913 K (1640 °C) and (f) 0.014 wt pct S at 1853 K (1580 °C).

As observed in a previous study by the authors [19] droplets with 0.007 wt pct S experienced phosphorus reversion when metal droplets entered the foamy slag; while for droplets with 0.014 wt pct S the reversion took place when the droplet was in transition between the dense and foamy slag. The dephosphorization behavior for a 0.007 wt pct S droplet without carbon is also shown in Figure 4(d) where the time scale is more than one order of magnitude higher than for the other five cases where the droplet contained carbon. No phosphorus reversion is observed in Figure 4(d) because there was no carbon to deplete FeO. Compared to carbon containing droplets, the dephosphorization rate is much lower in the case of carbon-free droplets as shown in Figure 4(d).

IV. DISCUSSION

A. Dephosphorization Kinetics of Carbon Free Droplets

Given the relatively high FeO content in the dense slag offering a relative high driving force and the fast FeO transport in dense slag, (based on the authors' previous work [14] k_{FeO} is 1.0×10^{-2} cm/s), the rate controlling step for carbon-free droplets is more likely to be mass transfer in metal phase. The integrated rate equation for phosphorus transfer in the metal can be expressed as Eq. [1]:

$$Ln\left[\frac{[\text{pct } P]_b-[pct\ P]_e}{[\text{pct } P]_o-[pct\ P]_e}\right]\left(\frac{[\text{pct } P]_o-[\text{pct } P]_e}{[\text{pct } P]_o}\right)\left(\frac{W_m}{\rho_m A}\right)=-k_m t \quad [1]$$

where W_m is the mass of the metal droplet, k_m is the mass transfer coefficient for phosphorus in the metal, ρ_m is the density of metal, $[\text{pct } P]_o$, $[\text{pct } P]_b$ and $[\text{pct } P]_e$ are the initial, bulk and equilibrium concentration of phosphorus in the metal.

Setting C = $\left[\frac{[\text{pct } P]_b - [\text{pct } P]_e}{[\text{pct } P]_o - [pct\ P]_e}\right]$ and B=$\left(\frac{[\text{pct } P]_o - [\text{pct } P]_e}{[\text{pct } P]_o}\right)\left(\frac{W_m}{\rho_m A}\right)$, Eq. [1] becomes B ln $C = -k_m t$

The data shown in Figure 4(d) was plotted in Figure 5 according to Eq. [1]. As seen in Figure 4(d), the phosphorus concentration [pct P] reaches a relatively constant value of 0.076 wt pct after 90 seconds which was chosen as $[\text{pct } P]_e$ in Eq. [1].

The slope of the line in Figure 5 represents the mass transfer coefficient of phosphorus in metal phase, k_m, which is 5.3×10^{-4} cm/s. This value for k_m is consistent with 6.7×10^{-4} cm/s measured by Zheng *et al.* [27] at 1783 K (1510 ^{o}C) and also shows a reasonable agreement with the finding from Rhamdhani *et al.* [28] where the mass transfer coefficients of aluminum in carbon free iron droplets was determined to be 1.3~1.9 ×10^{-4} cm/s in the temperature ranged from 1823 K (1550^{o}C) to 1923 K (1650 ^{o}C).

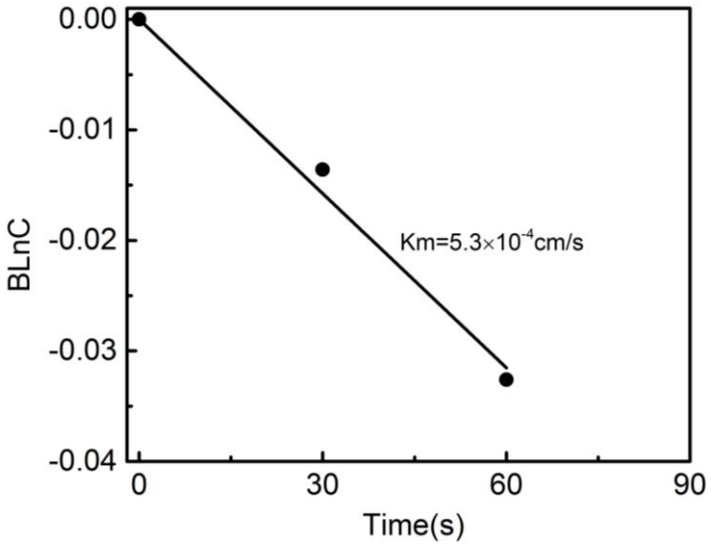

Fig. 5—Dephosphorization data from Fig. 4(d) is replotted based on Eq. [1].

The mass transfer coefficient for phosphorus in the metal, k_m, for carbon free droplets at 1853K (1580^{o}C) is two orders magnitude lower than that determined in Section B for droplets containing carbon under otherwise the same conditions. The high $k_m$values for carbon containing droplets appear to be related to the stirring provided by the formation of CO bubbles. Optical microscopy images of cross-sectioned droplets with and without carbon are shown in Figure 6. Figure 6(a) to (c) shows quenched samples of carbon containing droplets, which show a large fraction of large voids and many much smaller voids. These voids are the remnants of CO bubbles which appear to have collapsed and coalesced during quenching. No larger voids are observed in Figure 6(d) for carbon free droplets since CO evolution does not occur inside metal droplets, although some tiny voids are observed. This observation is consistent with the x-ray images.

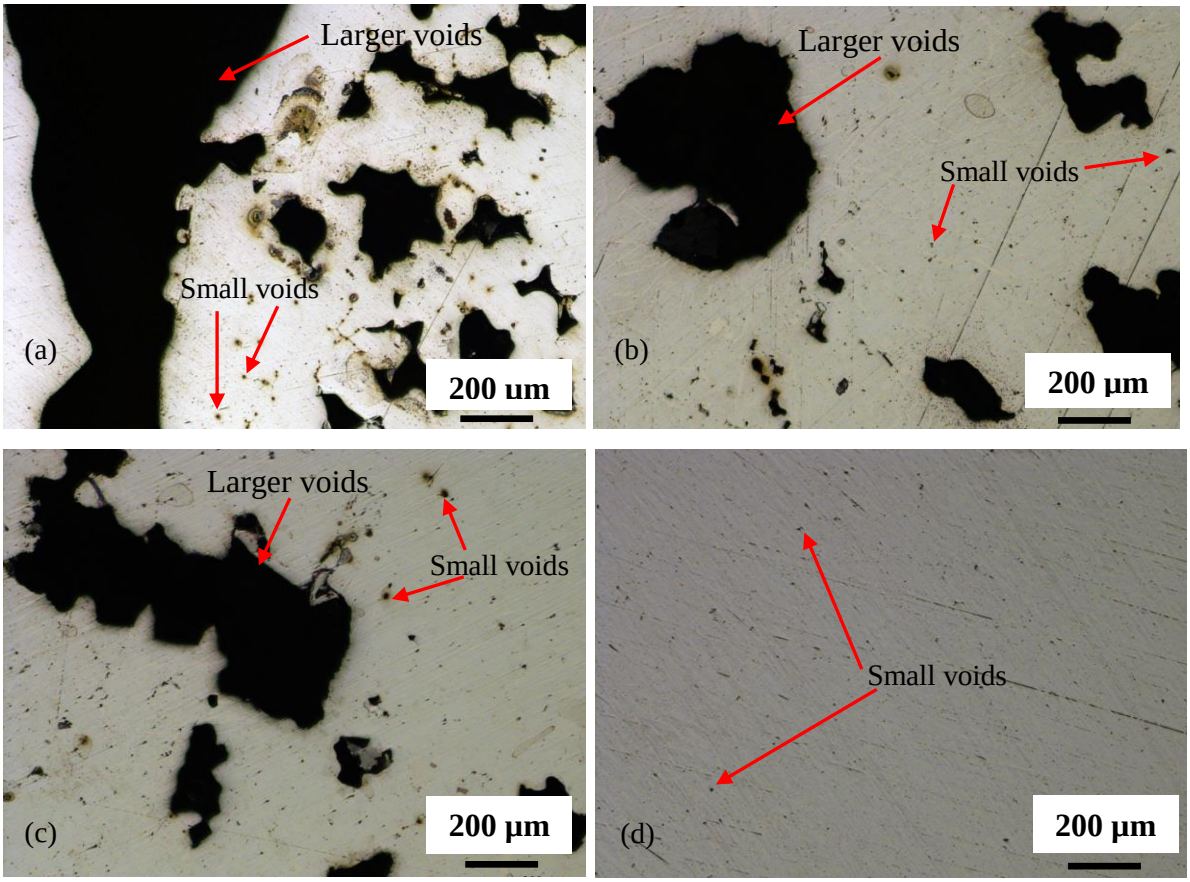

Fig. 6—Cross-section view of quenched droplets: (a) 0.007 wt pct S-1913 K (1640 °C), (b) 0.007 wt pct S-1853 K (1580 °C), (c) 0.007 wt pct S-1813 K (1540 °C) and (d) 0.007 wt pct S without C-1853 K (1580°C).

B. Dephosphorization Kinetics of Carbon Containing Droplets

In previous work by the authors, [19] it has been demonstrated that the rate of dephosphorization of bloated droplets prior to reversion was under mixed control by mass transfer in both metal and slag phase, as described by the following rate equation:

$$\left(\frac{W_m}{\rho_m A}\frac{1}{1+\frac{W_m}{L_P W_s}}\right) Ln\left[\left(1+\frac{W_m}{L_P W_s}\right)\frac{[\text{pct } P]_b}{[\text{pct } P]_o}-\frac{W_m}{L_P W_s}\right] = -k_o t \quad [2]$$

Using a similar approach to that for Eq. [1], setting C = $\left(1+\frac{W_m}{L_P W_s}\right)\frac{[\text{pct } P]_b}{[\text{pct } P]_o}-\frac{W_m}{L_P W_s}$ and B=$\left(\frac{W_m}{\rho_m A}\frac{1}{1+\frac{W_m}{L_P W_s}}\right)$, Eq. [2] becomes $B \ln C = -k_o t$. In Eq. [2], k_o, the overall mass transfer coefficient with the units of cm/s is defined as:

$$k_o = \frac{1}{\frac{\rho_m}{k_s \rho_s L_P}+\frac{1}{k_m}} \quad [3]$$

where k_s and k_m are the mass transfer coefficients for phosphorus in the slag and metal, ρ_m and ρ_s are the densities of metal and slag, L_P is the phosphorus partition coefficient.

All data for carbon containing droplets shown in Figure 4 were plotted in Figure 7 according to Eq. [2]. It is worth noting that as most of the dephosphorization is over within a few seconds, it is difficult to obtain enough data for meaningful kinetic plots as shown in Figure 7 with only two data points in some curves. The authors acknowledge this weakness, however, the data presented in Figure 7 show a remarkably consistent pattern where k_o decreases as temperature rises in the case of both 0.007 and 0.014 wt pct S droplets. The value of k_o drops by one order of magnitude as temperature increases from 1813 K (1540 °C) to1913 K (1640 °C).

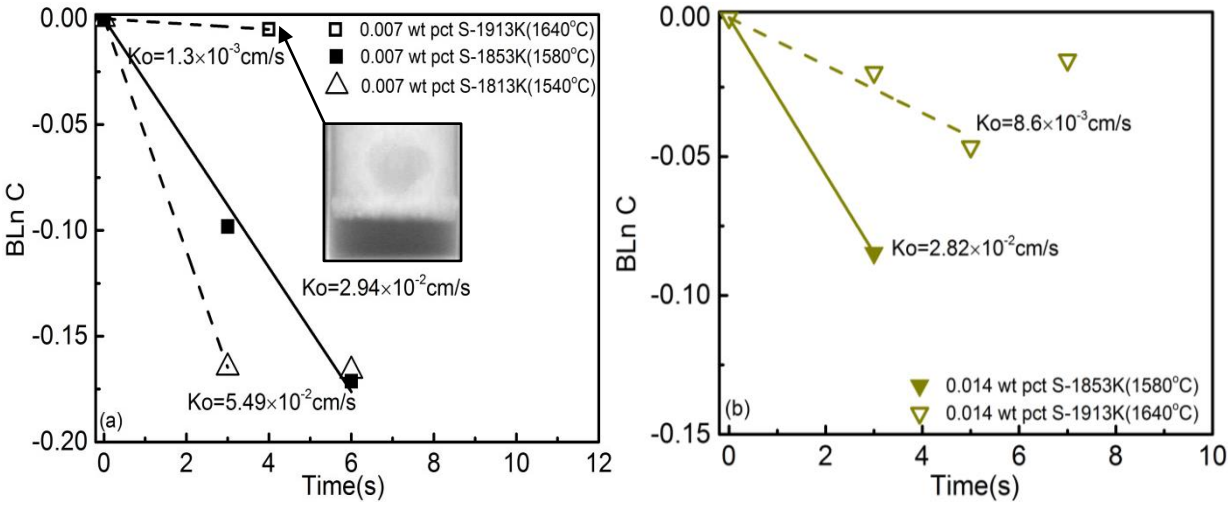

Fig. 7—Dephosphorization data from Fig. 4 are replotted as a function of time for different temperatures based on Eq. [2]: (a) 0.007 wt pct S and (b) 0.014 wt pct S.

Temperature affects three terms in Eq. [3], *i.e.*, k_s , L_P and k_m, leading to a change of k_o. In order to determine the most significant factor, the effects of temperature on k_s, L_P and k_m are evaluated in the following sections.

It is well known that the diffusivity in liquids is proportional to temperature but inversely proportional to viscosity according to the Stokes-Einstein and the Eyring equations:

$$D \propto \frac{T}{\eta} \quad [4]$$

Combining Higbie's penetration theory [29] with Eq. [4], one can obtain

$$k_s \propto (\frac{T}{\eta})^{1/2} \quad [5]$$

Therefore, knowing the viscosity of the slag as a function of temperature and the mass transfer coefficient, k_s, at one temperature, the values at other temperatures can be estimated. As shown in Figure 4, droplets with 0.007 wt pct S and 0.014 wt pct S are primarily dephosphorized in the

dense slag except for the case of 0.007 wt pct S at 1913 K (1640 ºC) which had the shortest incubation time. That special case will be discussed later. Assuming k_{FeO} is a reasonable estimate for k_s, results obtained from previous work by the authors may be employed. In the authors' previous work, [14] k_{FeO} in the dense slag was calculated to be 1.0×10^{-2}cm/s at 1853 K (1580 ºC). Determining the viscosity of slag for different temperatures using Factsage 6.4™ employing the Melts database, k_{FeO} under different temperatures was calculated and listed in Table I. It shows that the temperature effect on mass transfer coefficient k_{FeO} is negligible.

Table I: Calculated k_{FeO} at Different Temperature

T(K(ºC))	η /(poise)	$k_{FeO} \times 10^2$/(cm/s)	Initial Lp
1813(1540)	1.81	0.92	18
1853(1580)	1.49	1.01	13
1913(1640)	1.11	1.18	8

The initial value of L_P determined using Eq. [7] in combination with a method developed by the authors [14] to determine the interfacial oxygen potential is also presented in Table I. For completeness, this method, based on balancing the oxygen supply from reducible oxides in the slag and oxygen consumption by alloying elements in the metal, is described in detail in the Appendix. The data presented in Table I shows that the initial L_P decreases with increasing temperature. The phosphorus partition coefficient at the reversion point taken from Figure 4 is presented in Figure 8 as a function of temperature, which includes results from the work of Mori *et al*. [30] They investigated dephosphorization between liquid iron (Fe-3.6 wt pct C-0.1 wt pct P) and slag containing FeO. The related experimental conditions in their work including decarburization rate are listed in Table II. In addition, the current authors have added viscosities of different slags calculated using Factsage 6.4™ and maximum L_P calculated from reversion points as expressed in Eq. [6].

$$L_P = \frac{(\%P)_{max.}}{[\%P]_{min.}} \quad [6]$$

Knowing P_{O2}^i at t=0, the initial L_P (t=0) can be calculated based on Eqs. [7] and [8]. The initial L_P in the case of Mori *et al.* [30] were calculated and also listed in Table II.

$$L_P = \frac{(\%P)_i}{[\%P]_i} = \frac{C_{PO_4^{3-}} P_{O_2}^{i\ 5/4} f_P M_P}{K_P M_{PO_4^{3-}}} \quad [7]$$

where $C_{PO_4^{3-}}$ is the phosphate capacity of the slag, f_P is the henrian activity coefficient for phosphorus in the metal, M_P and $M_{PO_4^{3-}}$ are the molar mass of phosphorus and phosphate respectively, K_P is the equilibrium constant for the dissolution of phosphorus gas in steel.

In this study, phosphate capacity was determined based on the following correlation [31]:

$$\log C_{PO_4^{3-}} = 17.55\,\Lambda + \frac{51670}{T} - 21.867 \quad [8]$$

where Λ represents the theoretical optical basicity of slag, optical basicity values for individual oxides were taken from the literature. [32]

Table II: Slag Compositions (wt pct) and Extracted Results from Mori *et al.* [30]

No.	T/K(°C)	CaO	SiO_2	FeO	NaCl/(g)	η /(poise)	Max. L_P	Initial L_P	DeC. rate R×10^4/(mol/s)
A-4	1583(1310)	34.2	35.6	27.8		1.97	11.4	380.1	8.80
A-5	1573(1300)	34.2	35.6	27.8	1.0	1.21	32.2	270.1	8.84
B-9	1653(1380)	44.3	41.8	13.8		2.71	1.2	292.0	9.43
B-10	1653(1380)	44.3	41.8	13.8	2.0	0.95	9.0	116.6	13.6
C-6	1733(1460)	40.7	40.2	18.0		1.39	2.2	112.2	10.0
C-7	1723(1450)	40.7	40.2	18.0	1.0	0.93	3.2	76.8	11.8

Eq. [7] assumes that the activity coefficient of P_2O_5 is independent of P_2O_5 concentration. Turkdogan [33] demonstrated that at low concentrations of P_2O_5 (up to 1 wt pct) the activity coefficient is independent of temperature. In the current work although the maximum concentration of P_2O_5 in the slag is less than 0.02 wt pct the authors have accepted the temperature dependence proposed by Mori, [31] which has been well validated by experimental data.

In a study of dephosphorization equilibria between liquid iron and highly basic CaO-based slags saturated with MgO, Ishii and Fruehan [34] investigated the effect of Al_2O_3 additions by correlating the phosphate capacity of the slags with the theoretical optical basicity using Mori's correlation. [31] Although the theoretical optical basicity for slags used by Ishii and Fruehan [34] was higher than 0.73, the results fitted were well represented by Mori's correlation, [31] which was obtained in the range of optical basicity from 0.53 to 0.73. In a similar study to Ishii and Fruehan, [34] Li *et al.* [35] investigated the effect of Na_2O and Al_2O_3 on dephosphorization of molten steel using high basicity MgO saturated CaO-FeO_x-SiO_2 slag. They proposed a correlation that was qualitatively consistent with Mori's correlation [31] but predicted phosphate capacities which were an order of magnitude higher. Based on these observations and the agreement of Mori's correlation [31] for similar slag compositions to those in the current work, the authors have chosen to employ Eq. [8].

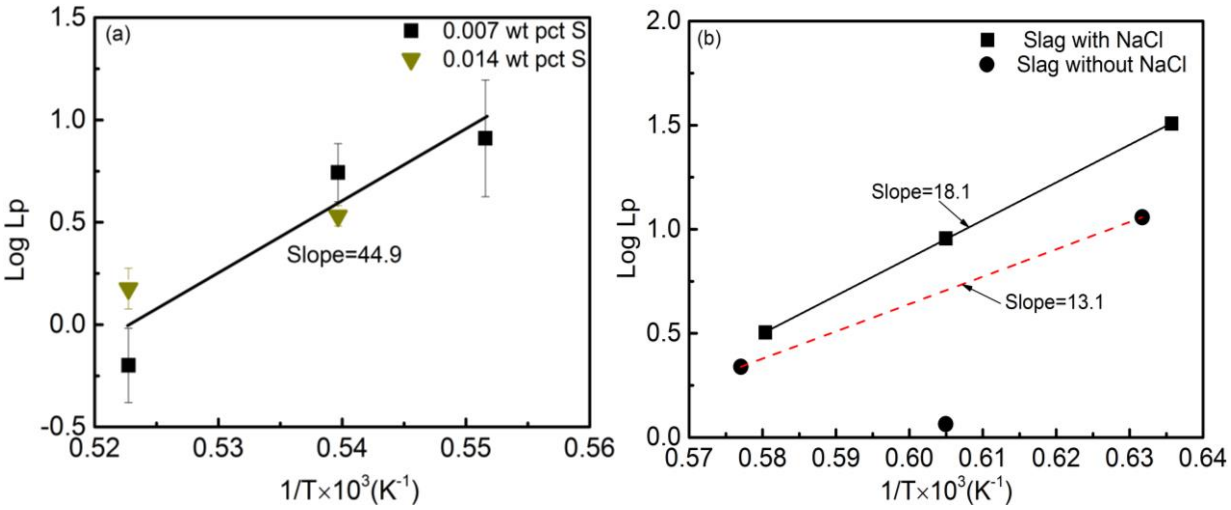

Fig. 8—The effect of temperature on phosphorus partition coefficient (L_P) at the reversion point: (a) this study and (b) calculated results using the data in the work of Mori *et al.* [30]

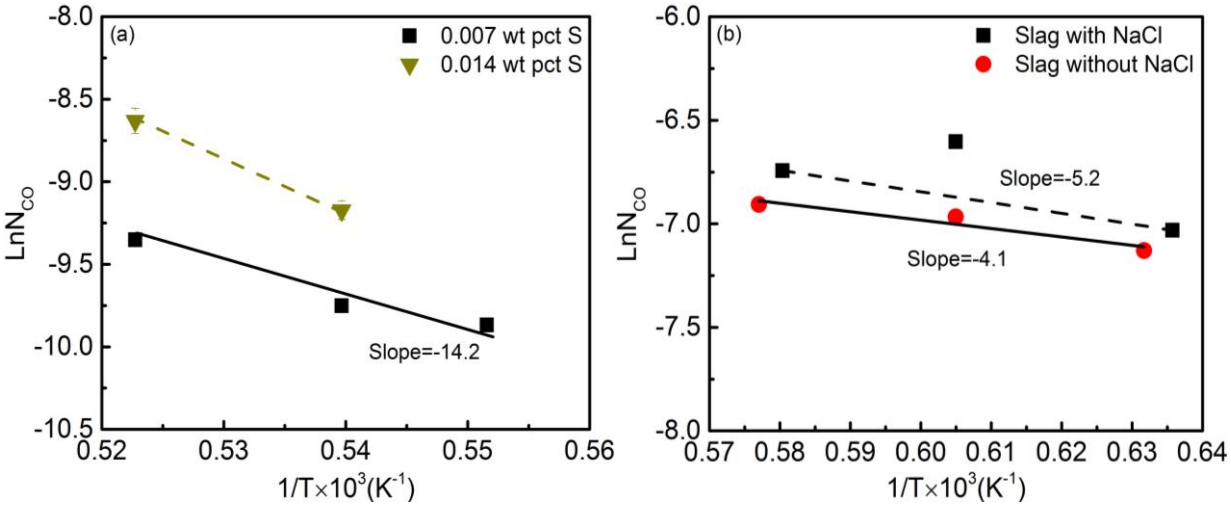

Fig. 9—Decarburization rate as a function of temperature: (a) this study and (b) calculated results based on the work of Mori *et al.* [30]

Figure 8 shows that the temperature coefficient of L_P for this study is different from that found in the work of Mori *et al.* [30] By examining Eq. [7], for a given slag composition the only term which the temperature dependency could change with specific circumstances is interfacial oxygen potential which decreases as decarburization proceeds. Although $\log C_{PO_4^{3-}}$ changes significantly with temperature, the deviation of temperature coefficient of L_P probably arises from the effect of decarburization. In order to understand the reason for the different temperature coefficients of L_P in this study and that of Mori *et al.*, [30] the decarburization rate as a function of temperature for each of these studies is plotted in Figure 9 according to an Arrhenius type expression, where N_{CO} is the maximum decarburization rate. The results for the 0.007 wt pct S droplets show a very good fit to the Arrhenius relationship, with apparent activation energy of 118 kJ/mol. This figure also

shows an apparent activation energy of 34.1 kJ/mol for the case of Mori *et al.*, [30] which is approximately one quarter of the value found in this study.

Taking the logarithm of Eq. [7] and separating each term, one can obtain:

$$\log L_P = \log C_{PO_4^{3-}} + \frac{5}{4}\log P_{O_2}^i - \log K_P + \log D \quad [9]$$

where $D = \frac{f_P M_P}{M_{PO_4^{3-}}}$, all are constants at given temperature.

The effect of each term in Eq. [9] on the temperature dependency of $\log L_P$ can be expressed as Eq. [10].

$$\frac{\partial \log C_{PO_4^{3-}}}{\partial \frac{1}{T}} = \frac{\partial \log L_P}{\partial \frac{1}{T}} - \frac{5}{4}\frac{\partial \log P_{O_2}^i}{\partial \frac{1}{T}} + \frac{\partial \log K_P}{\partial \frac{1}{T}} \quad [10]$$

The sum of RHS of Eq. [10] should be similar for this study and that of Mori *et al.*, [30] and equal to $\frac{\partial \log C_{PO_4^{3-}}}{\partial \frac{1}{T}}$, which is the same for all slags considered in this study. The temperature coefficient of interfacial oxygen potential can be estimated based on Eqs. [A3] (developed in the Appendix), [11] and [12]:

$$\begin{aligned}\log P_{O2}^i &= 2\log\left[\frac{\gamma_{FeO}K_{Fe}}{C_s * a_{Fe}^i * K_O}\left(C_{FeO}^o - \frac{1}{V_S}\int_{n_{CO},t=0}^{n_{CO},t=t} dn_{CO} - \frac{1}{A}\frac{1}{k_{FeO}}\frac{dn_{CO}}{dt}\right)\right] \\ &= 2\log\left(\frac{\gamma_{FeO}K_{Fe}}{C_s * a_{Fe}^i * K_O}\right) + 2\log\left(C_{FeO}^o - \frac{1}{V_S}\int_{n_{CO},t=0}^{n_{CO},t=t} dn_{CO} - \frac{1}{A}\frac{1}{k_{FeO}}\frac{dn_{CO}}{dt}\right)\end{aligned}$$

[11]

$$\frac{\partial \log P_{O_2}^i}{\partial \frac{1}{T}} = 2\frac{\partial \log\left(\frac{\gamma_{FeO}K_{Fe}}{C_s * a_{Fe}^i * K_O}\right)}{\partial \frac{1}{T}} + 2\frac{\partial \log\left(C_{FeO}^o - \frac{1}{V_S}\int_{n_{CO},t=0}^{n_{CO},t=t} dn_{CO} - \frac{1}{A}\frac{1}{k_{FeO}}\frac{dn_{CO}}{dt}\right)}{\partial \frac{1}{T}} \quad [12]$$

Setting E = $\frac{\partial \log\left(\frac{\gamma_{FeO}K_{Fe}}{C_s * a_{Fe}^i * K_O}\right)}{\partial \frac{1}{T}}$ and F= $\frac{\partial \log\left(C_{FeO}^o - \frac{1}{V_S}\int_{n_{CO},t=0}^{n_{CO},t=t} dn_{CO} - \frac{1}{A}\frac{1}{k_{FeO}}\frac{dn_{CO}}{dt}\right)}{\partial \frac{1}{T}}$, one can estimate E $\approx$ $\frac{\partial \log(K_{Fe})}{\partial \frac{1}{T}} - \frac{\partial \log(K_O)}{\partial \frac{1}{T}} = -12.5$ from the reported thermodynamic data, [36] which is same for this study and the case of Mori *et al.* [30] In current study, $C_{FeO}^o = 6.68 \times 10^{-3} mol/cm^3$, $\frac{1}{V_S}\int_{n_{CO},t=0}^{n_{CO},t=t} dn_{CO}$ is less than $4.5 \times 10^{-5} mol/cm^3$ estimated from Figure 2 from time zero to the time of phosphorus reversion for all the cases. Then this term $C_{FeO}^o - \frac{1}{V_S}\int_{n_{CO},t=0}^{n_{CO},t=t} dn_{CO}$ can be viewed as constant C. Knowing that $\ln(N_{CO}) = \frac{a}{T} + b$ from Figure 9 and the fact that k_{FeO} shows a negligible dependency on temperature established in earlier discussion, one can work out that

term F is essentially equal to $\frac{\partial \log\left(C-\frac{1}{Ak_{FeO}}\frac{1}{dt}\frac{dn_{CO}}{dt}\right)}{\partial \frac{1}{T}} \approx -\frac{\partial \ln(N_{CO})}{\partial \frac{1}{T}}$. Assuming this approach is also valid in the work of Mori *et al.* [30], then the value of each term in Eq. [10] can be determined by taking the slopes from Figures 8 and 9, which are listed in Table III.

Table III. Determined Temperature Coefficients for Terms in Eq. [10]

	$\frac{\partial \log C_{PO_4^{3-}}}{\partial \frac{1}{T}}$	$\frac{\partial \log L_P}{\partial \frac{1}{T}}$	$\frac{\partial \log P^i_{O_2}}{\partial \frac{1}{T}}$	$\frac{\partial \log K_P}{\partial \frac{1}{T}}$	Sum of RHS
This study	51.7	44.9	3.4	8.2	48.9
Mori *et al.* [30]	51.7	18.1	-14.6	8.2	44.6

From Table III, it can be seen that the sum of RHS of Eq. [10] are identical for this study and that of Mori *et al.* [30] and essentially equal to $\frac{\partial \log C_{PO_4^{3-}}}{\partial \frac{1}{T}}$, which shows that the deviation of temperature coefficient of L_P is related to the temperature effect on decarburization and thereby on oxygen potential.

C. Estimation of k_m at Different Stages of Reaction

Knowing k_o, L_P, k_{FeO} at different temperatures, it is worth employing Eq. [3] to calculate k_m at different temperatures. In the current study although L_P decreases as the reaction proceeds, the initial L_P may still be reasonably used to estimate the mass transfer coefficient during the initial stages of reaction, as shown in Figure 10.

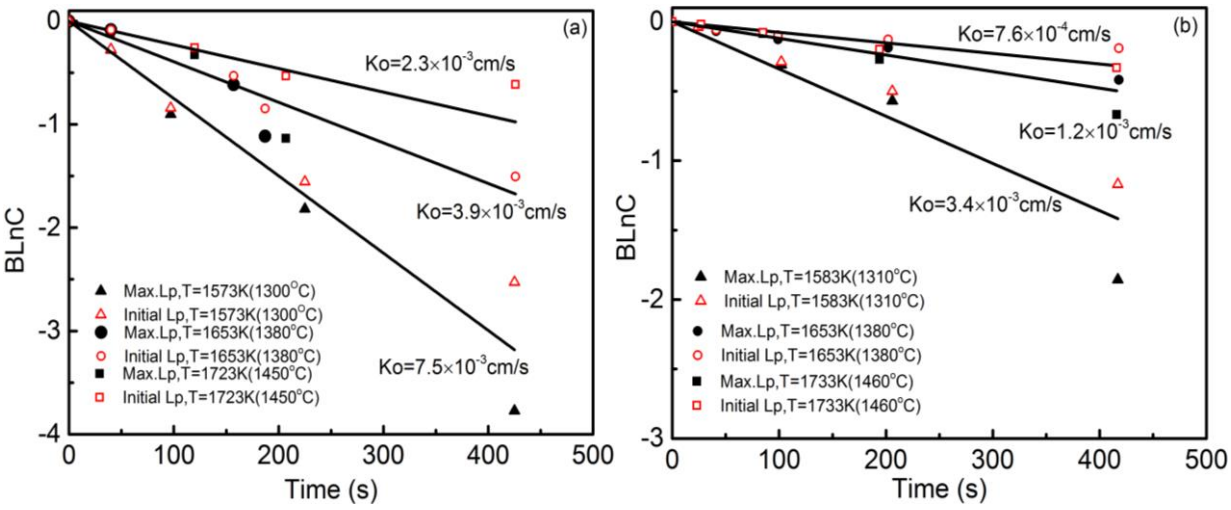

Fig. 10—Dephosphorization as a function of time and temperature plotted according to Eq. [2] using the data in the work of Mori *et al.* [30]: (a) slag with NaCl and (b) slag without NaCl.

The dephosphorization data from the work of Mori *et al.* [30] under the experimental conditions listed in Table II, were reproduced and replotted in Figure 10 according to Eq. [2]. The open data

points were calculated using initial L_P while the solid data points were obtained using maximum L_P. It shows that at the initial stage of reaction the data calculated based on initial L_P and maximum L_P overlap and can be fitted by a single line, which suggest that initial L_P can be used to determine the mass transfer coefficient without any significant loss of precision. k_m determined from k_o for a range of conditions is presented in Table IV for this study and Table V for the case of Mori *et al*. [30]

Table IV. Mass Transfer Coefficients Calculated from Experimental Data

T/(K(°C))	$k_o \times 10^2$/(cm/s) using max. Lp-0.007 wt pct S	$k_o \times 10^2$/(cm/s) using Initial Lp	$k_m \times 10^2$/(cm/s)-0.007 wt pct S	$k_o \times 10^2$/(cm/s) using max. Lp-0.014 wt pct S	$k_m \times 10^2$/(cm/s)-0.014 wt pct S
1813(1540)	5.49	3.32	24.57		
1853(1580)	2.94	2.25	6.16	2.82	5.65
1913(1640)	0.13	0.12	0.13	0.86	1.10

Table V. Mass Transfer Coefficients Calculated Using the Data in the Work of Mori *et al*. [30]

No.	T/K(°C)	$k_o \times 10^3$/(cm/s)	$k_m \times 10^3$/(cm/s)
A-4	1583(1310)	3.4	3.4
A-5	1573(1300)	7.5	7.5
B-9	1653(1380)	0.8	0.7
B-10	1653(1380)	3.9	4.1
C-6	1733(1460)	1.2	1.2
C-7	1723(1450)	2.3	2.3

Table IV and V show that the temperature has a strong effect on k_m in this study and the case of Mori *et al.* [30] where k_m decreases with increasing temperature. This result is contradicted by the general observation that mass transfer coefficients are usually increased as temperature rises. This contradiction appears to arise from the stirring effect introduced by the formation of CO bubbles inside the droplet, which varies with temperature.

In the current study, k_m can be estimated based on Higbie's penetration theory [29] which is expressed as:

$$k_m = 2\left(\frac{D\mu}{\pi d}\right)^{1/2} \quad [13]$$

where D is diffusivity (cm^2/s), of phosphorus in this case. [37] μ represents the velocity of the gas, which is CO evolution rate per unit area (cm^3/cm^2s). d is the average diameter of the CO bubbles (cm).

According to Eq. [13], if the size of CO bubbles is assumed to be independent of temperature within the temperature range investigated, one should expect a larger k_m at higher temperature due to the higher decarburization rate. Again this is contradicted by the results in Table IV and V. Therefore the only possible explanation is that the size of CO bubbles is smaller at lower temperature, leading to a faster surface renewal rate as predicted by Eq. [13], thereby offering a higher k_m, which will be addressed in detail in Section D.

The behavior of the droplets in this study is complex; the metal droplets first spent a short incubation time in dense slag before they bloat and float into the foamy slag, then, as bloating subsides, they sink back into the dense slag again. During this cycle, the control for dephosphorization changes from transport in both slag and metal to transport in the slag. The mixed control case has been evaluated in recent publications by the authors. [14, 19] To acquire a complete picture of droplet refining, it is necessary to estimate the phosphorus mass transfer coefficient in the metal phase, k_m, at different stages, *i.e.*, high decarburization rates (bloated droplet) and low decarburization rates (dense droplet). At 1913 K (1640 ºC) k_m for 0.007 wt pct S droplets seems unreasonably low compared with that for 0.014 wt pct S droplets especially if one consider those two have similar k_o and k_m values at 1853 K (1580 ºC), as shown in Table IV. Inspection of X-ray images reveals that the metal droplet is floating in the foamy slag as shown in Figure 7, which suggests that k_o in the case of 0.007 wt pct S droplet at 1913 K (1640 ºC) represents, or at least partially represents, mass transfer in foamy slag. This would lead to an error in determining k_m based on the assumption of a k_s value representative of dense slag. To make a more reasonable estimate of k_m it is possible to make use of the similarity between mass transport in the metal for the 0.007 wt pct S and 0.014 wt pct S case. Table IV shows that k_m for 0.007 wt pct S (6.16×10^{-2}cm/s) and 0.014 wt pct S (5.65×10^{-2}cm/s) are similar at 1853 K (1580ºC), *i.e.*, $(\frac{\mu}{d})^{1/2}_{0.007wt\ pctS} \approx (\frac{\mu}{d})^{1/2}_{0.014wt\ pctS}$ according to Eq. [13]. If one assumes the same relationship exists at 1913 K (1640 ºC), the initial k_m of dense droplet in the case of 0.007 wt pct S droplet can be recalculated to be 1.60×10^{-2} cm/s by knowing CO gas evolution rate from Figure 2. This recalculated value is listed in Table VI, which also includes parameters used to estimate k_m for bloated droplets in the foamy slag based on Eq. [13]. The initial value of k_m for a dense droplets based on Figure 7 is also presented in Table VI.

The calculated values of k_m for bloated droplets in foamy slag shows that if one assumes no growth of CO bubbles during the course of the experiment, k_m in foamy slag is slightly smaller than the initial k_m for dense droplets due to the larger surface area as shown in Table VI. Although the bloated droplets have higher decarburization rate, the effect of increased surface area off-sets the effect of higher CO generation rate.

Table VI: Parameters for Calculating k_m of 0.007 wt pct S Bloated Droplets in the Foam

Parameter	1813K(1540 °C)	1853K(1580 °C)	1913K(1640 °C)
Initial DeC. rate*10^5/(mol/s)	2.47	2.73	6.52
Peak DeC. rate*10^5 /(mol/s)	5.18	5.82	7.28
End DeC. rate*10^5 /(mol/s)	0.1~1.0	0.1~1.2	0.1~1.0
Initial average A/(cm^2)	1.32	1.40	1.56
Peak average A/(cm^2)	7.71	6.87	7.67
End average A/(cm^2)	1.32	1.51	1.37
Diffusivity*10^5 /(cm^2/s) [37]	1.86	2.14	2.62
$k_m * 10^2$ /(cm/s) of bloated droplet	14.7	4.05	1.33
Initial $k_m * 10^2$ /(cm/s) of dense droplet	24.6	6.16	1.60*

*Recalculated value based on Eq. [13].

From Figures 4(a), (b), (c) and (e), it can be seen that metal droplets experienced renewed dephosphorization on falling back into the dense slag, especially in the case of Figure 4(a) and (b). In both of these cases there is sufficient data to analyze the kinetics of this second period of dephosphorization. Since the droplet continued to form CO gas as it sank into the dense slag, it is reasonable to assume that the reaction of dephosphorization was controlled by mass transfer in both metal and slag phase but without the depletion of FeO due to the relative lower decarburization rate as shown in Table VI. Therefore, the data from Figures 4(a) and (b) at the point where renewed dephosphorization starts are replotted in Figure 11 based on Eq. [2]. The time plotted starts from the time the droplet is estimated to have dropped back into the dense slag. The initial phosphorus was taken at the same time.

After the droplet sinks back into the dense slag, the rate controlling step for dephosphorization shifts to mass transfer in both metal and slag phase again. This shift is due to the higher concentration of FeO in dense slag, leading to a relative higher k_o, *i.e.*, 1.07×10^{-2} cm/s and 1.28×10^{-2} cm/s as shown in Figure 11. Knowing the k_{FeO} and L_P for dense slag listed in Table I, k_m during the final stage for 0.007 wt pct S droplets was calculated and is shown in Table VII.

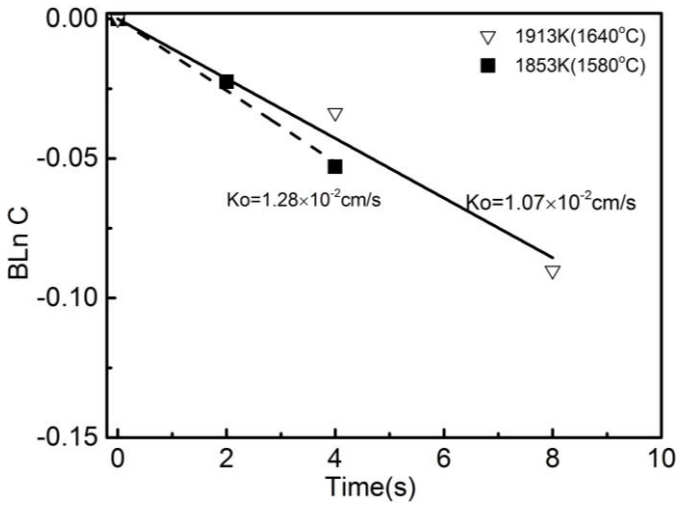

Fig. 11—Redephosphorization data from Fig. 4(a) and (b) are replotted as a function of time via Eq. [2].

Table VII. Calculated k_m at Different Stages

T(K(°C))	$k_m \times 10^2$/(cm/s) at initial stage	$k_m \times 10^2$/(cm/s) in the foam	$k_m \times 10^2$/(cm/s) at final stage
1813(1540)	24.6	14.7	
1853(1580)	6.16	4.05	1.66
1913(1640)	1.60*	1.33	1.46

*Recalculated value based on Eq. [13].

Table VII shows that k_m at the final stage of reaction was lower than that during the incubation period for decarburization, due to the weaker stirring in the final stage with much lower decarburization rate as shown in Table VI. For example, at 1853 K (1580 °C), the decarburization rate during the initial stage is approximately 4 times higher than the average value at the end, which would lead to a higher k_m value by at least a factor of 2 according to Eq. [13]. That is to some extent consistent with the results in Table VII, *i.e.*, k_m is 6.16×10^{-2} cm/s at initial stage and 1.66×10^{-2} cm/s at the end.

All mass transfer coefficients including k_o, k_m and k_{FeO} are summarized in Figure 12, which shows that during the life of a bloated droplet the controlling step for dephosphorization changes. In dense slag corresponding to initial dephosphorization stage and re-dephosphorization stage, the rate is under mixed control by mass transfer in both metal and slag phase. The values of k_o sits in the range between k_m and k_s, except for the case of initial dephosphorization at 1913 K (1640 °C) where the value of k_o is lower and close to k_s. One possible explanation for the latter observation, is that since the measured k_o for this case shown in Figure 7(a) does not represent k_o for initial dephosphorization in dense slag as it does for the other conditions, but is based on the renewed dephosphorization which might alter the values of both k_s and k_m. The overall mass transfer coefficient k_o is slightly higher during the initial stage of dephosphorization compared with

renewed dephosphorization which occurs when the decarburization reaction is almost over. This observation may be attributed the larger mass transfer coefficient for phosphorus in the metal caused by the higher decarburization rate during the initial period. While in the foamy slag, the rate control is found to be mass transfer in the slag at which k_o is approximately equal to k_{FeO} in the foamy slag. The shift to control by mass transport in the slag may be attributed to the low phosphorus partition caused by the combined effect of a lower k_{FeO} in the foamy slag, depletion of FeO from the limited liquid volume of the foamy slag and the high decarburization rate associated with bloating. These factors would lead to the rate controlled by mass transport in the slag. In the present case we have assumed that $k_{FeO}= k_s$, however it seems unlikely that the mass transport of phosphate in the slag would be as fast as that of oxygen (nominally treated as FeO). In the absence of a better estimation we have chosen to use k_{FeO}.

The dash line in Figure 12 shows the calculated pathway of overall mass transfer k_o during the reaction. k_o is initially high but decreases due to the decreasing interfacial oxygen potential as decarburization proceeds and the metal droplet moves from the dense slag to the foamy slag. This stage has been successfully modeled, at a single temperature, in previous work by the authors. [14] That work shows excellent agreement with the current results. It should be recognized that in the case of droplets in a real BOF the slag will be foamy for the residence time of the droplet, and over the life of an individual droplet the FeO content of the slag will remain essentially constant. These factors will change the trajectory of k_o presented in Figure 12 however the insights developed in this work and the results obtained should be sufficient to allow prediction of dephosphorization for a droplet by droplet basis in a kinetic model of the BOF. On going work in the authors' laboratory is aiming to embed the current kinetic data in a holistic model of the BOF.

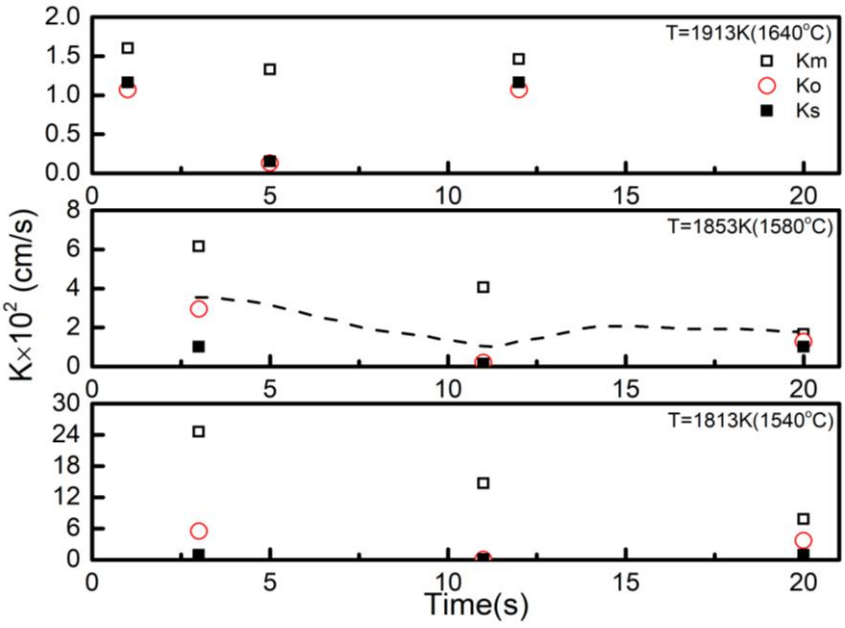

Fig. 12—Mass transfer coefficients for the whole life of bloated droplet.

D. The Effect of Temperature on k_m

Based on the above discussion, the only possible explanation for the higher k_m at lower temperature in this study is that the CO bubbles are smaller at lower temperatures, leading to a faster surface renewal rate as predicted by Eq. [13], thereby offering a higher k_m. For the nucleation of CO bubbles, the relationship between the pressure inside the critical nucleus and its' radius r^*can be estimated from Young-Laplace equation:

$$\Delta P = (P_{ve} - P_l) = \frac{2\sigma}{r^*} \quad [14]$$

where in the case of CO bubble nucleation, P_{ve} is the pressure in the bubble at equilibrium (supersaturation pressure), P_l is the liquid pressure (1atm), σ represents the surface tension of liquid metal. Due to the high supersaturation pressure for CO nucleation, $(P_{ve} - P_l) \approx P_{ve}$. It is worth noting that there is no change in ferrostatic pressure in the current work. In the BOF, the atmospheric pressure in the vessel may change with time. However, the supersaturation pressure based on calculated activities of carbon and oxygen is about 125 atm which will render any pressure change in a real BOF negligible.

If the formation of CO bubbles follows reaction [15], [36]

$$[C] + [O] = CO_g \quad [15]$$

$$\Delta G^o = -22200 - 38.34T\ (J/mol) \quad [16]$$

Then the equilibrium constant can be written as:

$$K_{15} = \frac{P_{ve}}{h_C h_O} \quad [17]$$

where h_C and h_O are the henrian activity of carbon and oxygen in liquid metal.

Combing Eqs. [14] and [17], one can obtain,

$$r^* = \frac{2\sigma}{K_{15} h_C h_O} \quad [18]$$

Considering the negligible temperature effect on activity of carbon and oxygen for a given metal compostion, [36] the change of CO bubble critical size mainly arises from the change of the equilibrium constant. According to Eq. [16], as temperature increases the equilibrium constant, K, decreases. The surface tension for liqiuid iron containing sulfur in the range considered in the current study also inreases with temperature. Both the aforementioned effects lead to a larger critical radius. The smaller CO bubbles which form at lower temperature offer a faster surface renewal thereby leading to a higher mass transfer coefficient as observed in Table VII.

Combining Eqs. [13] and [18], the following equation can be derived:

$$k_m = \left(\frac{h_C h_O D \mu}{\pi \sigma} K_{15}\right)^{1/2} \quad [19]$$

k_m is plotted in Figure 13 according to an Arrhenius type expression based on the values presented in Table VII and V for this study and the case of Mori *et al*. [30]

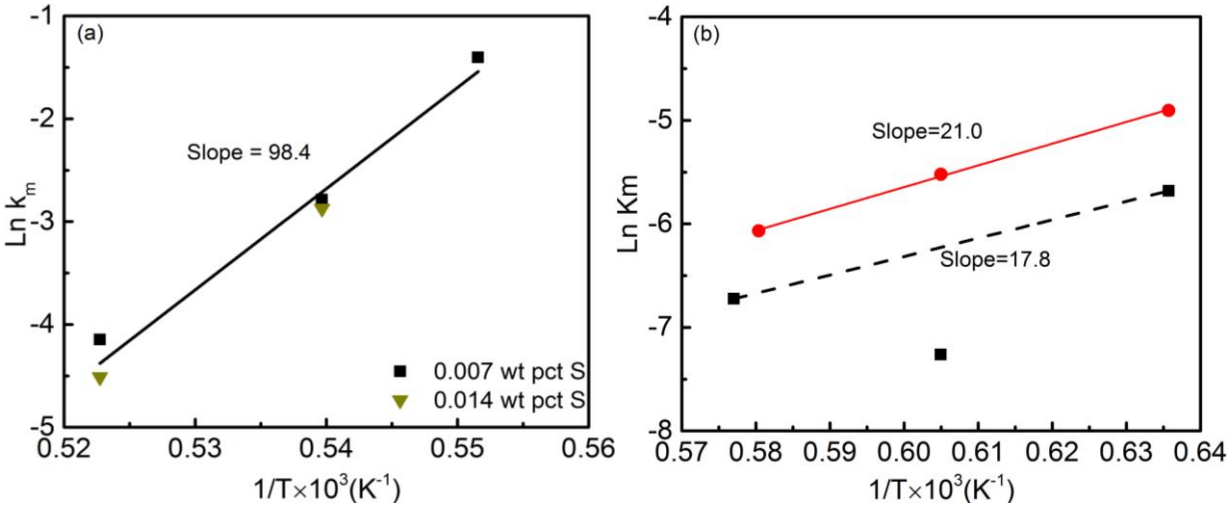

Fig. 13—The plot of k_m as a function of temperature: (a) this study and (b) calculated results based on the work of Mori *et al*. [30]

It can be seen that in Figure 13 the apparent activation energy in this study is approximately 5 times higher than that from the work of Mori *et al*. [30] This result is consistent with the results from Figure 9 where the apparent activation energy for decarburization in this study is 4 times higher than that in the case of Mori *et al*. [30]

Again, taking the logarithm of Eq. [19] and separating each term, one can obtain:

$$\ln k_m = \frac{1}{2}(\ln K_{15} + \ln \mu - \ln \sigma + \ln D + \ln P) \quad [20]$$

where $P = \frac{h_C h_O}{\pi}$ is assumed to be a constant since the change of h_C, h_O with temperature is negligible in comparison to the other terms considered in Eq. [20].

The relationship between the temperature dependencies of all terms in Eq. [20] can be expressed as Eq. [21].

$$\frac{\partial \ln K_{15}}{\partial \frac{1}{T}} = 2\frac{\partial \ln k_m}{\partial \frac{1}{T}} - \frac{\partial \ln \mu}{\partial \frac{1}{T}} - \frac{\partial \ln D}{\partial \frac{1}{T}} + \frac{\partial \ln \sigma}{\partial \frac{1}{T}} \quad [21]$$

Setting $M_1 = \left(2\frac{\partial \ln k_m}{\partial \frac{1}{T}}\right)_1 - \left(\frac{\partial \ln \mu}{\partial \frac{1}{T}}\right)_1 - \left(\frac{\partial \ln D}{\partial \frac{1}{T}}\right)_1$ and $N_1 = \left(\frac{\partial \ln \sigma}{\partial \frac{1}{T}}\right)_1$, and similar terms can be written for M_2 and N_2, where subscript 1 and 2 represent this study and the case of Mori *et al*., [30] respectively.

Since $\frac{\partial \ln K_{15}}{\partial \frac{1}{T}}$ is $\frac{-\Delta H}{R}$ for reaction [15] and should have the same value for both cases, then one would expect the sum of RHS of Eq. [21] for this study and the case of Mori *et al.* [30] should equal the LHS of Eq. [21]. By reading values from Figures 9 and 13, one can obtain M_1=222 and M_2=58, where M_1 is approximately 4 times higher than M_2 which suggests N_1 is to be smaller than N_2, *i.e.*, the temperature coefficient of surface tension in this study should be smaller than the one in the case of Mori *et al.* [30]

Chung and Cramb [22] investigated the effect of sulfur and temperature on the surface tension of Fe-4 wt pct C alloys, and developed the following equation to calculate the surface tension as expressed in Eq. [22], where the temperature was extended to 1913K (1640°C) for this study.

$$\sigma = 1913 + 0.43[1823 - T] + 67.75[\text{pct } C] - 0.107T[\ln 1 + K_S a_s] - 0.153T[\ln 1 + K_O a_O] \quad [22]$$

where K_S and K_O are the adsorption coefficients for sulfur and oxygen respectively in liquid-iron alloys, a_s and a_O are activities of sulfur and oxygen, which can be calculated based on interaction coefficients. [36]

There is a possibility that the surface tension will change with time because of changes in droplet chemistry. However, changes in the sulfur content will be negligible given the slag basicity (wt pct CaO/wt pct SiO_2=0.9) and the oxygen potential (~$10^{-9.4}$ atm). The interfacial oxygen activity does change with time so it is likely that the oxygen potential inside the droplet will change. However, in analyzing the effect of surface tension on the temperature dependency, it was necessary to choose a specific condition. Given that the mass transfer coefficient is constant over the time period considered, one may assume that any unaccounted for change of surface tension has not introduced a significant error.

Based on Eq. [22], without sulfur and oxygen the temperature coefficient of surface tension for pure iron is -0.43. Therefore $N_2=\left(\frac{\partial \ln \sigma}{\partial \frac{1}{T}}\right)_2$ for the case of Mori *et al.* [30] was calculated to be 0.52. In this study where metal droplets contain 0.007 wt pct S and 0.014 wt pct S and around 0.005 wt pct O [19, 28], N_1 was calculated to be -6.46 and -7.36 for 0.007 and 0.014 wt pct S droplets, respectively. Taking the average value of -6.91, N_1 is around 10 times lower than N_2. Even assuming liquid iron in the work of Mori *et al.* [30] has the same amount of oxygen 0.005 wt pct O as this study; N_2 was calculated to be -2.67, which is still more than 2 times higher than N_1.

From above calculation, the sums of RHS of Eq. [21] for this study and the case of Mori *et al.* [30] are 215 and 58.5, respectively, which shows that in neither the current study nor the work of Mori *et al.* [30] does the RHS of Eq. [21] yield standard formation enthalpy of CO (-22.2 kJ/mol) [36] within a reasonable experimental error. The authors are not able to offer an explanation for this except to note that Chen and Coley [23] and Kwak and Oh [38] pointed out that the nucleation of CO

in this case does not follow classical nucleation theory. If that is indeed the case Eq. [19] may require additional terms that have not been included.

In this study, the authors have proposed that high mass transfer coefficients for phosphorus in metal phase may be attributed to stirring inside the metal droplet caused by internal evolution of CO. One may argue that it is unlikely to form CO nuclei inside metal droplet due to a very high supersaturation requirement. However, CO formation inside the droplet is supported by experimental observation in the current work as shown in Figure 3 (droplet swelling) and in several other studies. [6, 7] It is also shown, in at least three separate studies in our lab, that the CO generation rate is proportional to droplet mass. [6, 7, 39] The only explanation for these observations is that the gas nucleates homogeneously (or pseudo-homogeneously) within the droplet. Despite its theoretical "impossibility", the authors suggest that the fact of CO gas nucleating inside droplets is well established. [23, 38, 40-44]

E. Industrial Relevance

In this study, 1 g droplets with a diameter of 6.4 mm were used for experimental convenience. Ciccutti *et al.* [45] reported the diameter of droplets sampled from the BOF ranged from 0.23 to 3.35 mm. A range between 0.16 and 3.36 mm was also reported by Meyer *et al.* [46] The diameter of 6.4 mm used in the current study is above average diameter of droplets found in the BOF. However, according to several previous studies in the authors' laboratory [6, 7, 39] the CO evolution rate within the droplet has been found to scale with the droplet volume, therefore the decarburization rate can easily be determined for smaller droplets. Because the CO evolution rate controls the mass transfer of phosphorus, the dephosphorization rate can be calculated for smaller droplets and within reason for larger droplets where the internal nucleation is likely to hold. The authors have recently prepared a draft manuscript detailing the effect of droplet size on dephosphorization kinetics. [39] That paper shows that the methodology presented in the current paper, for dealing with mass transport can readily accommodate different droplet diameters over the range (7.4mm > d > 5mm). Although it is not experimentally feasible to use smaller sizes the mechanism of mass transport should allow scaling to the sizes relevant to the BOF.

In the authors' view the most significant finding of this paper is that for all sized droplets the dephosphorization rate is fast (complete in < 6 seconds) relative to the residence time of the droplet (a few seconds to 60 seconds for bloated droplets). The overall dephosphorization rate may be calculated at any time during the blow by knowing the local equilibrium partition and the rate of droplet generation. The authors are currently working to build this finding into an overall model of the BOF.

V. CONCLUSION

The effects of temperature on the dephosphorization kinetics of bloated metal droplets containing 0.007 and 0.014 wt pct S, was investigated in detail by employing a mixed mass transfer control model in the temperature range from 1813 K (1540 °C) to 1913 K (1640 °C). The mass transfer

coefficient of phosphorus in the metal, k_m, affected by CO gas stirring at different stages of reaction was estimated by combining the penetration theory with a model for nucleation of CO. Metal droplets without carbon were also studied to elucidate the effect of decarburization on dephosphorization. The pathway of the overall mass transfer coefficient k_o for dephosphorization was evaluated over the whole course of reaction. Finally, the effect of temperature on k_m was investigated for a temperature range of 1813 K (1540 ^{o}C) to 1913 K (1640 ^{o}C). The following conclusions can be drawn from the current study.

1. In this study, the rate controlling step of dephosphorization for metal droplets without carbon is mass transfer of phosphorus in the metal phase, and k_m is calculated to be 5.3×10^{-4}cm/s, which is two orders of magnitude lower than that for carbon containing droplets.

2. For droplets containing carbon, the analysis of dephosphorization kinetics shows that the overall mass transfer coefficient, k_o, decreases with increasing temperature due to the enhanced decarburization, which reduces the phosphorus partition ratio by lowering the dynamic interfacial oxygen potential.

3. The mass transfer coefficient for phosphorus in the metal, k_m, for carbon bearing droplets is also found to decrease with increasing temperature because the size of CO bubbles are larger at higher temperature which decreases the rate of surface renewal.

ACKNOWLEDAGMENTS

The authors thank member companies in McMaster Steel Research Centre and the Natural Science and Engineering Research Council of Canada (NSERC) for funding this project.

REFERENCE

1. E. W. Mulholland, G. S. F. Hazeldean and M. W. Davies: *J. Iron Steel Inst.*, 1973, vol. 211, pp. 632-39.
2. T. Gare and G.S.F. Hazeldean: *Ironmak. Steelmak.*, 1981, vol. 4, pp. 169-81.
3. H. Gaye and P.V. Riboud: *Metall. Trans. B*, 1977, vol. 8B , pp. 409-15.
4. D.J. Min and R.J. Fruehan: *Metall. Trans. B*, 1992, vol. 23B, pp. 29-37.
5. C.L. Molloseau and R.J. Fruehan: *Metall. Trans. B*, vol. 33B, 2002, pp. 335-44.
6. E. Chen: PhD Thesis, McMaster, Hamilton, CA, 2011, pp.59-79.
7. M. Pomeroy: Master Thesis, McMaster, Hamilton, CA, 2011, pp.42-66.
8. G. A. Brooks, Y. Pan, Subagyo and K.Coley: *Metall. Trans. B*, 2005, vol. 36B, pp. 525-35.
9. Subagyo, G.A. Brooks, and K. Coley: *Can. Metall. Quarterly*, 2005, vol. 44 (1), pp119-29.
10. N. Dogan, G. A. Brooks and M. A. Rhamdhani: *ISIJ Int.*, 2011, vol. 51 (7), pp. 1086-92.
11. N. Dogan, G. A. Brooks and M. A. Rhamdhani: *ISIJ Int.*, 2011, vol. 51 (7), pp. 1093–01.
12. G. Brooks, B. Rout, A. Rhamdhani and Z. Li: *CAMP-ISIJ*, 2015, vol.28, pp. 509-12.
13. A. K. Hewage, B. K. Rout, G. Brooks and J. Naser: *Ironmak. Steelmak.*, 2016, vol. 43 (5), pp. 358-70.
14. K. Gu, N. Dogan and K. Coley: *Metall. Trans. B*, 2017, DOI: 10.1007/s11663-017-1000-2.
15. P. Wei, M. Ohya, M. Hirasawa, M. Sano and K. Mori: *ISIJ.Int.*, 1993, vol. 33 (8), pp. 847-54.
16. P. Wei, M. Sano, M. Hirasawa, and K. Mori: *ISIJ Int.*, no. 3, vol. 33 (3), 1993, p. 479-87.

17. E. Shibata, H. Sun and K. Mori: *Metall. Trans. B*, 1999, vol. 30B, pp. 279-86.
18. B. J. Monaghan, R.J. Pomfret, and K.S. Coley: *Metall. Trans. B*, 1998, vol. 29B, pp. 111-18.
19. K. Gu, N. Dogan and K. Coley: *Metall. Trans. B*, 2017, DOI: 10.1007/s11663-017-1002-0.
20. Z. Li, K. Mukai, M. Zeze and K. C. Mills: *J. Mater. Sci.*, 2005, vol. 40, pp. 2191-95.
21. K. Nakashima and K. Mori: *ISIJ Int.*, 1992, vol. 32 (1), pp. 11-18.
22. Y. Chung and A. Cramb: *Metall. Trans. B*, 2000, vol. 31B, pp. 957-71.
23. E. Chen and K. Coley: *Ironmak. Steelmak.*, 2010, vol. 37 (7), pp. 541-45.
24. C. P. Manning and R. J. Fruehan: *Metall. Trans. B*, 2013, vol. 44B, pp. 37-44.
25. A. Assis, J. Warnett, S. Spooner, R. Fruehan, M. Williams and S. Sridhar: *Metall. Trans. B*, 2015, vol. 46B, pp. 568-76.
26. S. Spooner , A. Assis, J. Warnett, R. Fruehan, M. Williams and S. Sridhar: *Metall. Trans. B*, 2016, vol. 47B, pp. 2123-32.
27. S. Zheng, W. Chen, J. Cai, J. Li, C. Chen and X. Luo: *Metall. Trans. B*, 2010, vol. 41B, pp. 1268-72.
28. M. A. Rhamdhani, G. A. Brooks and K. S. Coley: *Metall. Trans. B*, 2005, vol. 36B, pp. 219-27.
29. R. Higbie: Trans. *Am. Inst. Chem. Eng*., 1935, vol. 31, pp. 365-89.
30. K. Mori, Y. Fukami and Y. Kawai: *Trans. ISIJ*, 1988, vol.28, 315-18.
31. T. Mori: Trans. *Jpn. Inst. Met.*, 1984, vol. 25 (11), pp. 761-71.
32. V. D. Eisenhuttenleute: Slag Atlas, 2nd editions, 1995, pp. 10-19.
33. E. T. Turkdogan: *ISIJ Int.*, 2000, vol. 40 (10), pp. 964-70.
34. H. Ishii and R. J. Fruehan: *ISS Trans.*, February, 1997, pp. 47-54.
35. G. Li, T. Hamano and F. Tsukihashi: *ISIJ Int.*, 2005, no. 1, vol. 45, pp. 12-18.
36. M. Hino and K. Ito: Thermodynamic Data for Steelmaking, Tohoku University Press, Sendai. 2009, pp. 259-64.
37. Y. Kawai and Y. Shiraishi: Handbook of Phyico-chemical Properties at High Temperatures, 1988, Chapter 7, pp. 196.
38. H. Kwak and S. Oh: *J. Colloid interface Sci.*, 1998, vol. 198, pp.113-18.
39. K. Gu, N. Dogan and K. Coley: *Metall. Trans. B*, 2017, Unpublished research.
40. S. D. Lubetkin: *Langmuir*, 2003, 19, pp. 2575-87.
41. N. H. Ei-Kaddah and D. G. Robertson, *J. Colloid interface Sci.*, 1977, vol. 60, pp. 349-60.
42. K. S. Coley, E. Chen and M. Pomeroy: Celebrating the Megascale, Wiley, 2014, pp. 289-02.
43. H. S. Levine: *Metall. Trans. B*, 1973, vol. 4B, pp. 777-82.
44. H. S. Levine: *Metall. Trans. B*, 1974, vol. 5B, pp. 953-55.
45. C. Ciccutti, M. Valdez, T. Perez, J. Petroni, A. Gomez, R. Donayo and L. Ferro: 6th Int. Con. on Molten, Slags, Fluxes and Salts, 2000, paper367.
46. H. W. Meyer, W. F. Porter, G. C. Smith and J. Szekel: *JOM*, 1968, July, pp.35-42.

APPENDIX

In the authors' previous study, [14] it was shown that by balancing the oxygen supply from reducible oxides in the slag and oxygen consumption by carbon in the metal, the P_{O_2} at the interface between slag and liquid metal can be determined via Eq. [A1].

$$k_{FeO}\left(C_{FeO}^{b} - C_{FeO}^{i}\right) = \frac{1}{A}\frac{dn_{CO}}{dt} \quad [A1]$$

Here, $\frac{dn_{CO}}{dt}$ is the CO generation rate (mole/s), C_{FeO} is the concentration of FeO, A is the surface

area of the droplet, k_{FeO} describes oxygen transport in the slag conceptually defined as the mass transfer coefficient for FeO. C_{FeO}^{i} may be expressed in terms of activity of oxygen at the interface and C_{FeO}^{b} expressed as a function of the initial concentration of FeO modified by the amount reduced (dn_{FeO}). If one makes these substitutions, and further recognizes that dn_{FeO} is equivalent to the amount of CO generated (dn_{CO}), one may rearrange Eq. [A1] to obtain Eqs. [A2] and [A3].

$$P_{O2}^{i} = \left[\frac{\gamma_{FeO}K_{Fe}}{C_s * a_{Fe}^{i} * K_O}\left(C_{FeO}^{b} - \frac{1}{A}\frac{1}{k_{FeO}}\frac{dn_{CO}}{dt}\right)\right]^2 \quad [A2]$$

$$P_{O2}^{i} = \left[\frac{\gamma_{FeO}K_{Fe}}{C_s * a_{Fe}^{i} * K_O}\left(C_{FeO}^{o} - \frac{1}{V_s}\int_{n_C,t=initial}^{n_C,t=t} dn_{CO} - \frac{1}{A}\frac{1}{k_{FeO}}\frac{dn_{CO}}{dt}\right)\right]^2 \quad [A3]$$

where K_{Fe} and K_O are the equilibrium constants for FeO dissociation and oxygen dissolution in iron; γ_{FeO} is the activity coefficient for FeO in the slag, C_s is the overall molar density of the slag and V_S is the volume of slag. The term, $C_{FeO}^{o} - \frac{1}{V_s}\int_{n_C,t=initial}^{n_C,t=t} dn_C$, represents the FeO content of the slag at time t. It is important to note that V_s must be defined as either the volume of dense slag or the foamy slag depending on the location of the droplet.

The middle term, $\frac{1}{V_s}\int_{n_C,t=initial}^{n_C,t=t} dn_C$, in Eq. [A3] describes the amount of carbon oxidized, which is taken from experimental measurements. To use this equation for a specific reaction time one will be required to calculate the concentration of FeO. This instantaneous FeO concentration can be calculated from the initial concentration of FeO and the amount of carbon oxidized between time zero and time t. Using the X-ray videos one can calculate the volume of foamy slag and dense slag at any given time, thereby determining the amount of liquid slag in each phase. Assuming no mixing between the two after the droplet is in the foamy slag, one can calculate the change in FeO for the foamy slag.